

## Characterization of air outgassing process in dye degradation experiments using hydrodynamic jet cavitation

### Charakterisierung von Luftausgasung bei Experimenten zum Farbstoffabbau mittels hydrodynamischer Strahlkavitation

**J.-A. Nöpel, M. Krieger, E. Frense, F. Rüdiger**

Institute of Fluid Mechanics (ISM), Technische Universität Dresden, Germany

Jet cavitation, dye degradation, outgassing, shadowgraphy, bubble spectra  
Strahlkavitation, Farbstoffabbau, Ausgasung, Schattenverfahren, Blasenspektren

#### Abstract

The paper presents an investigation of bubble spectra downstream of a cavitation reactor caused by outgassing. This is of interest because the existence of bubbles potentially has an influence on the chemical reactivity of the jet cavitation. To investigate the influence, a correlation of experiments on dye degradation and bubble analysis is drawn. The oxidative effect of cavitation was previously demonstrated by dye degradation studies. For a configuration with a small nozzle diameter of  $d = 0.6$  mm the best degradation rates were achieved at a pressure difference of  $\Delta p = 40$  bar. Furthermore, no increase in degradation could be found with an increase in back pressure. The configuration of high degradation is particularly characterized by a low gauge back pressure ( $p_2 = 0.07$  bar) and thus notably strong outgassing in the reactor. The outgassed air bubbles were quantified in a transparent analysis section downstream the reactor. As pressure difference  $\Delta p$  increases, the number and size of the bubbles increases. Rising back pressure leads to a significant decrease in the number of bubbles. For the operating condition with the highest dye degradation, bubbles of  $d = 70 - 320$   $\mu\text{m}$  were detected. Degradation rates above optimal pressure difference decrease, while at the same time the number of large bubbles with  $d > 200$   $\mu\text{m}$  increases significantly. Basically, a large number of small outgassed bubbles is of positive influence on the degradation.

#### Introduction

Cavitation is defined as local pressure reduction down to vapor pressure with subsequent pressure increase. This results in the dynamic growth of bubbles, which is terminated by an increase in pressure. The implosion of the bubbles lead to locally extremely high pressure and temperature. These conditions cause a homolytic cleavage of water forming radicals. The radicals are able to randomly oxidize substances in water. Such processes are called advanced oxidation processes (AOP) (Munter, 2001).

Hydrodynamic cavitation is a widely considered aspect of research, which on the one hand deals with the negative effects on components and processes. On the other hand, the usable positive aspects for processing and water treatment are increasingly being researched and optimized (Braeutigam et al. 2012). It turns out that often the fluid mechanical aspects in the reactor are assumed as a black box and so reactive properties of a cavitating flow are not

optimized. This leads to difficulties since cavitation is primarily a fluid mechanical phenomenon, which influences the chemical-reactive part on the basis of various parameters. Mostly, the dependency of local conditions in the reactor such as bubble distribution and size or collapse intensity on process parameters are not investigated.

The paper deals with the correlation of results of dye degradation experiments (Nöpel et al., 2021) using hydrodynamic cavitation and air outgassing due to jet cavitation. The study includes investigations with two nozzles at different pressure boundary conditions. In the configurations investigated, it becomes apparent that the air outgassing process occurs stronger as pressure difference increases, while this can be minimized with increasing back pressure.

Therefore, the influence of process conditions is investigated based on analysing the air bubble content in water flow downstream of the reactor using shadowgraphy. It is hypothesized that by increasing the outgassing intensity due to increasing pressure difference, the AOP process can be intensified. In addition, it is postulated that there is a transition point at which the gas bubble loading becomes too high so that damping of bubble collapse and subsequently degradation rates becomes significant.

## Experimental setup

In the experiment, demineralized water flows through an inlet tube into a cavitation reactor (1) via a nozzle and forms a jet in the reactor chamber. The setup is shown in Figure 1. Depending on the pressure difference between the high pressure in the inlet pipe  $p_1$  and the back pressure in the reactor  $p_2$ , flow velocities are reached which lead to hydrodynamic cavitation with air outgassing. By adjusting the pressure boundary conditions via adjustable high-pressure pump (6) and control valves (3), the bubble density and collapse intensity in the reactor can be varied. The pump provides a flow rate up to  $\dot{V} = 10$  l/min and operating pressure up to  $p_{\max} = 100$  bar. In this study pressure differences of up to  $\Delta p = 60$  bar are investigated.

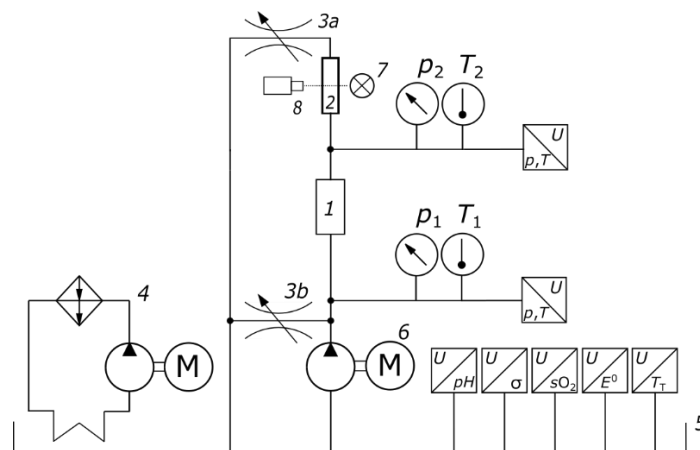


Figure 1: Hydraulic circuit of the experimental setup: 1 – reactor chamber with cavitating jet, 2 – transparent analysis section for bubble detection, 3 – control valve (3a for back pressure regulation, 3b for bypass control), 4 – cooling system, 5 – open tank with process measuring equipment, 6 – in-line piston pump, 7 – backlight, 8 – camera

Deionized water flows in the closed loop of stainless steel piping system. During the experiments, measurements were performed with two nozzles:  $d = 0.6$  mm and  $d = 1.0$  mm. The volume of the reactor was  $V_R = 9000$  mm<sup>3</sup> with a square cross-sectional area of  $A_R = 900$  mm<sup>2</sup>. For optical accessibility, the reactor has acrylic walls. The water temperature has kept constant in the range of  $T = (25 \pm 2)$  °C during the measurements. The total fluid volume in the circuit amounted to  $V = 2$  l. The circuit has an open tank where the process measurement equipment is implemented. In the tank, parameters as pH-value, conductivity  $\sigma$ , oxygen saturation  $sO_2$ ,

temperature  $T$  and redox potential  $E^0$  are continuously measured. These quantities are essential to verify reproducibility and to ensure comparability of the results.

### Measurement techniques and data evaluation

For the dye degradation experiments, a solution of Congo red (CAS: 573-58-0, from Alfa Aesar) with a concentration of  $c_0 = 30$  mg/l was filled into the system. The pump run for several system volume passages before starting the experiment. This ensures homogeneous distribution of the dye in the system, while during this period no cavitation occurred. Hereafter, the first sample was taken from the tank to determine the initial concentration. Afterwards the operating point to be investigated was set and the treatment procedure started for a period of 60 minutes. Long-term tests without cavitation showed no change in dye concentration. The dye concentration of the samples was analyzed using a spectrophotometer (Genesys 10S UV-Vis).

Through the results of the dye degradation the question arises which conditions lead to a particularly effective degradation. For this purpose, the bubble distribution and the cavitating jet length were investigated in previous studies (Deggelmann et al. 2022, Nöpel et al. 2018). With increasing pressure ratio, independent on nozzle diameter, the jet penetration depth increases until it is limited by the length of the reactor and the number of bubbles due to outgassing increased. In this work, the focus is on the bubbles originated by outgassing. In the paper of Nöpel et al. 2021, it was already shown that with decreasing nozzle diameter the oxygen saturation of the processed water decreases. The quantification of the air volume fraction by the detected spherical bubbles in the transparent analysis section will indicate the strength and the influence of the outgassing.

The analysis section shown in Figure 2 is used to capture the air bubbles downstream of the reactor (2). It has a depth of  $t = 2$  mm, a width of  $b = 16$  mm and a height of  $h = 100$  mm and allows optical accessibility through transparent acrylic viewing windows. Figure 2 shows this component together with the measuring equipment for shadow method. For image acquisition, a camera from Bresser (MikroCamII 5MP HIS Microscope Camera) with 5 MP (1) is positioned in front of the section. The image resolution is  $2048 \times 2048$  px<sup>2</sup> for an area of  $16 \times 16$  mm<sup>2</sup>. For backlight illumination, an opal glass (3) for homogenization of the light and high power LED (LED Head - LPS v3, ILA\_5150) (4) are installed.

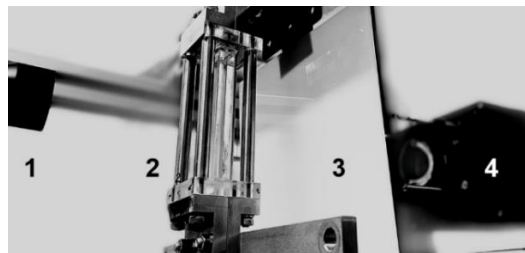


Figure 2: Configuration for bubble detection by shadow method, consisting of 1 – camera, 2 – transparent analysis section, 3 – opal glass and 4 – high-power LED

The camera was used to record videos over a period of  $t = 3$  min, from which 179 images were extracted and analyzed. The starting point for the selection of several image processing algorithms is the work of Mickler, 2014. Based on Mickler, two algorithms were considered the most efficient according to the prevailing experimental constraints - the Hough Transform (HT) and the Euclidean Distance Transform (EDT). These two algorithms were implemented using the open source programs and packages Python (PyCharm), Anaconda, OpenCV, Scikit-Image and Plotly. The HT and EDT algorithms were both evaluated. The EDT algorithm leads to more accurate results in bubble detection and has a slightly increased runtime compared to the HT algorithm. The EDT algorithm was selected as the primary choice for the bubble detection. The

input medium is the recorded video. Based on the video a background image using Median Background Subtraction (MBS) is created and used in the image analysis procedure. For each second one image is analysed, see Figure 4, left. Figure 3 shows the workflow diagram.

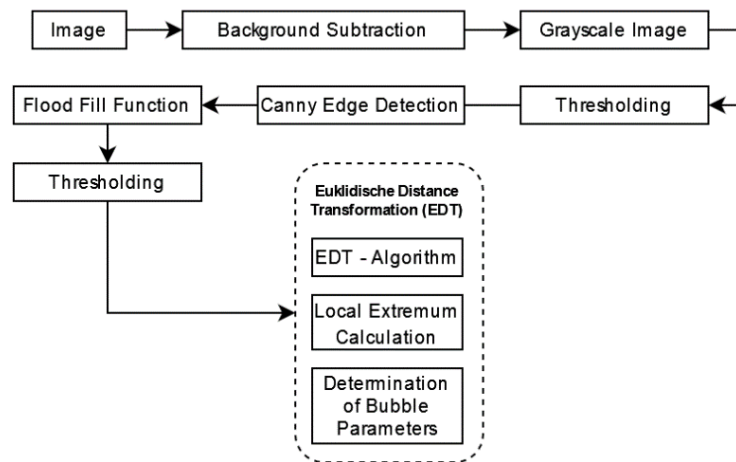


Figure 3: Workflow diagram for bubble detection with Euclidean distance transformation

The grayscale picture is the result from the image subtraction of the analysed picture from the background picture. It follows thresholding and blurring implementations to prepare the image for the Canny Edge Detection. This is a prerequisite for the flood-fill function which is necessary for filling the bigger bubbles resulting from the recording process. Through additional thresholding the image is converted to a binary image. The EDT algorithm detects the various bubbles present (Figure 4, right) in the picture and calculates their centre point and radii. The thresholding value and images size is being retained to guarantee comparable findings across all survey points.

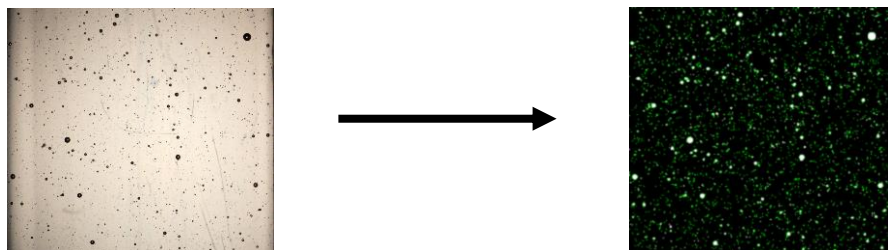


Figure 4: Bubble detection in the transparent analysis section: Left: Original image; Right: Image of detected bubbles

## Results of dye degradation experiments

In a previous paper, the effect of the cavitating jet in the reactor with different nozzle diameters and pressure differences was investigated. The cavitating flow in terms of process engineering application, process optimization and reproducibility of the experiment was similarly considered. For this purpose, degradation experiments were conducted with the dye Congo red (Nöpel et al. 2021). It was found that the degradation and energy consumption ratio tended to be optimal for small nozzles. A correlation was found between the degradation ratio and the oxygen saturation at the equilibrium state of the process. Figure 5 left displays the results of the degradation experiments with different nozzle sizes and pressure differences dependent on change of oxygen saturation caused by the treatment. It becomes apparent that the saturation change is greatest for the smallest nozzle, which is due to outgassing.

The graph on the right side of Fig. 5 shows degradation ratio over hydraulic power  $P$ . Here, the three power levels stand for pressure differences of  $\Delta p = \{20, 40, 60\}$  bar. It is obvious that

an effective operating point prevails for the configurations at  $\Delta p = 40$  bar. Additionally, it is shown that degradation with smaller nozzle was measured 1.5 times higher and degradation decreases with further increasing power input.

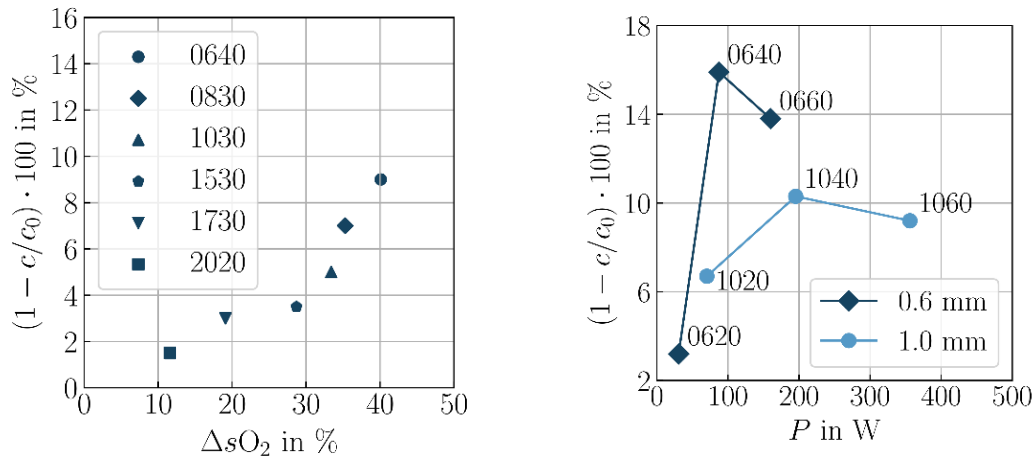


Figure 5: Results of dye degradation experiments; Left: Degradation ratio of Congo red in percent compared to oxygen saturation in percent due to cavitation processing for different nozzle and pressure difference configurations at constant number of system volume passages  $N_{svp} = 35$  and equal use of hydraulic energy  $E = 0.35$  MJ (Nöpel et al. 2021); Right: Change of degradation at different power levels with  $d = 0.6$  mm and  $d = 1$  mm; calculation of power  $P (= \Delta p \cdot V / t_r)$  with  $V / t_r$  the volume flow and energy  $E (= \Delta p \cdot V)$ . Configuration labelling example – 0660: First two numbers indicate nozzle size:  $d = 0.6$  mm; last two numbers indicate pressure difference:  $\Delta p = 60$  bar; points connected by linear trend lines

Starting from the most effective operating points of the nozzles, Figure 6 shows results of increasing back pressure  $p_2$ . Increasing back pressure forces bubble collapse, shortens area of cavitating jet and significantly reduces the number of outgassed air bubbles in the reactor chamber and so in the pipe system downstream.

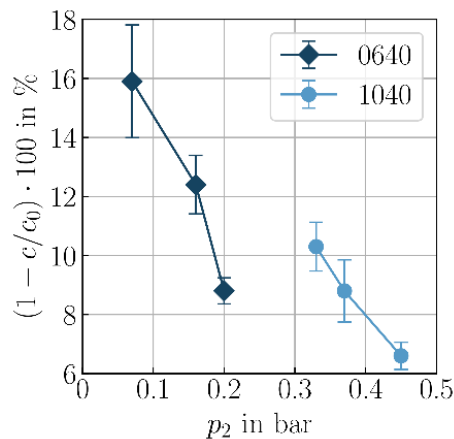


Figure 6: Degradation results of nozzles with  $d = 0.6$  mm and  $d = 1$  mm at  $\Delta p = 40$  bar with different back pressure  $p_2$ ; points connected by linear trend lines

For both nozzles, degradation reduces significantly with increasing back pressure. In principle, pressure gradients, shear intensity, degree of turbulence, jet length, back pressure and hence the strength of outgassing varies for different operating points in the reactor. In the following, the outgassing will be quantified on the basis of the amount and spectra of bubbles downstream the reactor, to indicate the state of the flow more clearly and to specify the influence of outgassing.

## Flow conditions and bubble properties

In order to characterize the different flow conditions of the cavitating flow, three dimensionless similarity numbers are given in Table 1 for the different configurations with  $d = 1$  mm and  $d = 0.6$  mm: Reynolds number  $Re$ , cavitation number  $Ka$  and Thoma number  $Th$ . While the  $Re$  reflects the ratio of frictional to viscous forces and  $Ka$  provides a classification of cavitation intensity, the Thoma number reflects the ratio of inlet to back pressure at the reactor. Low  $Th$  refers to a lower probability of outgassing because of high back pressure.

Table 1: Overview of dimensionless numbers for the operating conditions investigated; Reynolds number  $Re$ , cavitation number  $Ka$ , and Thoma number  $Th$ .

Configuration	$Re = w_d \cdot d / \nu$	$Ka = (p_\infty - p_v) / (0.5 \rho w_d^2)$	$Th = p_1 / p_2$
0620	33,604	0.07	461
0640	46,520	0.03	545
0660	56,560	0.02	580
1020	56,007	0.10	120
1040	77,535	0.05	121
1060	94,268	0.03	120

In the following the bubble amount and bubble spectra detected in a video sequence of  $t = 180$  s are presented. During the measurement, pressure difference, temperature, oxygen saturation and  $pH$  were kept constant. The amount of bubbles reported represent the total amount of bubbles detected out of 179 images. The bubble spectra contain the total amount of detected bubbles sorted by classes of radii. The minimum cut-off radius was set to  $r_B = 70$   $\mu\text{m}$ . This value results from preliminary investigations on the detectability of bubbles. Figure 7 displays the total amount of detected bubbles  $N$  for the investigated operation points of  $d = 0.6$  mm and  $d = 1$  mm. In Figure 7, left,  $N$  is plotted over power  $P$ . The maximum number of air bubbles for both nozzles occurs for  $\Delta p = 40$  bar.

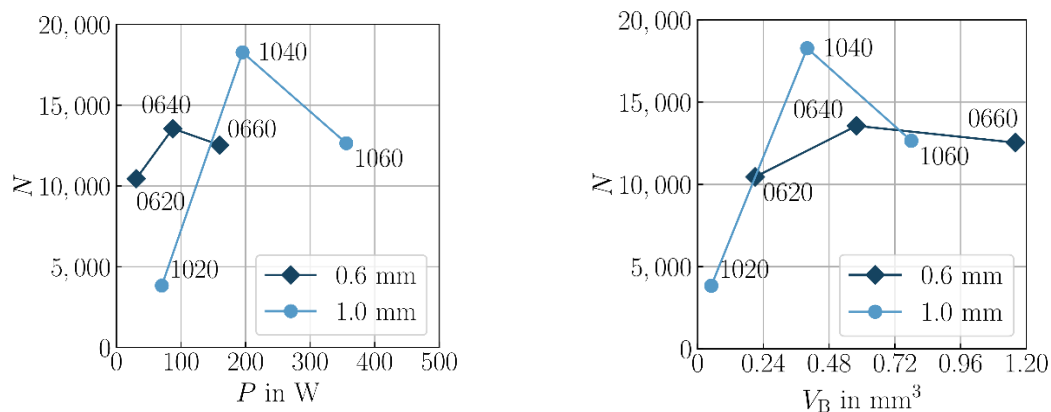


Figure 7: Total number of detected bubbles  $N$  for the three investigated operating points  $\Delta p = \{20; 40; 60\}$  bar with  $d = 0.6$  mm and  $d = 1$  mm; Left: Plot of  $N$  over power  $P$ ; Right: Plot of  $N$  over air volume  $V_B$  from total bubble amount; points connected by linear trend lines

For  $d = 1$  mm, the maximum total amount of detected bubbles is  $N = 18,273$  and is thereby higher by a factor of 1.3 than for the maximum with  $d = 0.6$  mm. In Figure 7, right, the total amount of bubbles is shown over the total air bubble volume  $V_B$ . It is obvious that a maximum of bubbles exists at  $\Delta p = 40$  bar, but the bubbles are larger at  $\Delta p = 60$  bar and thus contain more air. In comparison between the amount of bubbles, it turns out that the air volume is higher for each comparable operating point using smaller nozzle. Degradation results from Figure 5 correlate with those of total bubble number in Figure 7. The degradation of dye for both nozzles is maximum where the bubble number of small bubbles is maximum. Higher pressure

difference above  $\Delta p = 40$  bar results in lower degradation rate because of maximum amount of air volume due to bubbles.

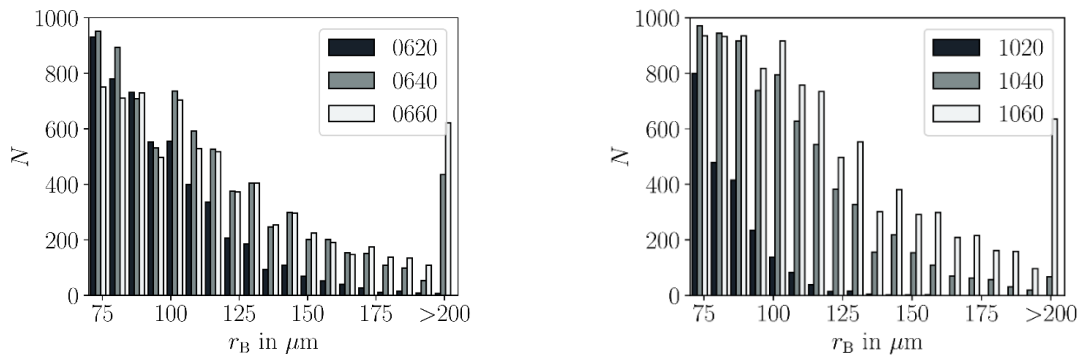


Figure 8: Histograms illustrating the bubble size spectra in terms of bubble radii in  $\mu\text{m}$  for the three operating points investigated; Left: nozzle with  $d = 0.6$  mm; Right: nozzle with  $d = 1$  mm

Figure 8 shows two histograms displaying the bubble size spectra for the three operating points investigated. Bubbles were detected at each operating point. It is evident that for the smaller nozzle fewer bubbles were detected in the range below  $r_B = 200 \mu\text{m}$  compared to  $d = 1$  mm. This may be because of a significant number of bubbles below the detection range of  $r_B = 70 \mu\text{m}$  or of coalescence of smaller bubbles inside the reactor chamber and will be a part of further investigation. Based on the  $> 200 \mu\text{m}$  class, the greater the pressure difference, more larger bubbles were formed. The change of the total amount of bubbles over the three operating points is stronger for  $d = 1$  mm. Especially at operating point 1060, a high amount of bubbles  $> 200 \mu\text{m}$  was recorded.

Finally, the results on the influence of the increase of the back pressure  $p_2$  are presented. Figure 9 left shows the total number of bubbles with increasing back pressure. For both nozzles there is significant decrease in the amount of bubbles. Increasing the back pressure is therefore a way of minimizing outgassing. The dye degradation (see Figure 6), as well as the bubble amount significantly decreases with increasing back pressure.

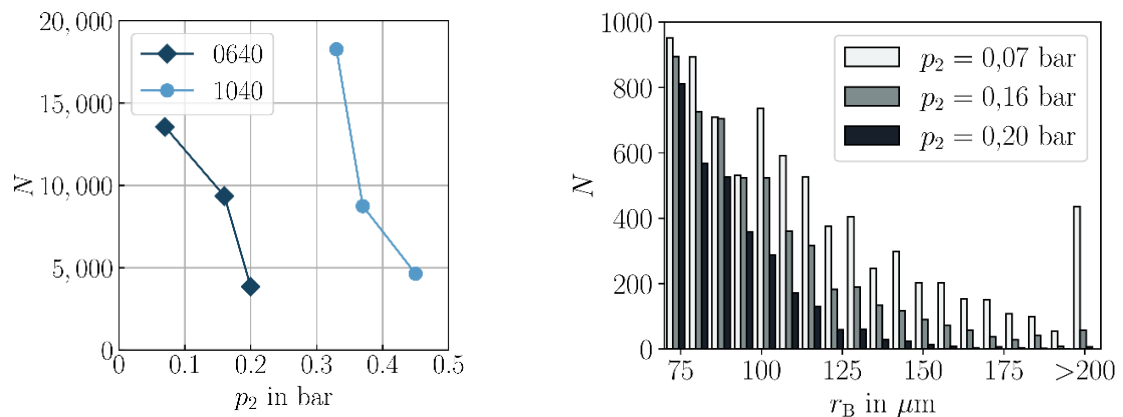


Figure 9: Detected bubbles  $N$  with  $d = 0.6$  mm and  $d = 1$  mm at  $\Delta p = 40$  bar and varying back pressure  $p_2$ ; Left: Total amount of bubbles over back pressure; Right: Histograms, illustrating the bubble size spectra in terms of bubble radii in  $\mu\text{m}$  for  $d = 0.6$  mm; points connected by linear trend lines

The effects of increasing back pressure is displayed in Figure 9 right by the change of bubble size spectra. For the configuration with  $d = 0.6$  mm, the naturally occurring back pressure due to the pipe resistance is  $p_2 = 0.07$  bar. For both nozzles, at  $\Delta p = 40$  bar, the number and size of air bubbles decrease significantly with increasing back pressure. If  $p_2$  would be increased more than four times natural resistance pressure, the total amount of bubbles will drop down

to zero detection events minimizing outgassing in the reactor. But it turns out that this also influences dye degradation and minimises it.

### Concluding remark

The paper presented results of dye degradation experiments and an evaluation of the amount of air bubbles downstream a cavitation reactor recorded by shadowgraphy. The bubble images were analyzed by Euclidian distance transform gaining bubble size spectra.

It was found that the dye degradation is highest with smaller nozzle at  $d = 0.6$  mm. At  $\Delta p = 40$  bar, for the reactor used a particularly efficient operating point is found. The dye degradation for the 0640 configuration was 16 % in a treatment time of 60 min. With the larger nozzle with  $d = 1$  mm, the degradation at operating point 1040 was comparatively low at 10 %. The power used for operating point 0640 was less by a factor of 2.2, this configuration thus is more efficient. For both nozzles, an increase of the back pressure  $p_2$  resulted in a significant reduction of the dye degradation.

### Literature

**Braeutigam, P.; Franke, M.; Schneider, R.; Lehmann, A.; Stolle, A.; Ondruschka, B., 2012:** "Degradation of carbamazepine in environmentally relevant concentrations in water by hydrodynamic-acoustic-cavitation", *Water Research*. 10.1016/j.watres.2012.02.013.

**Deggelmann, M; Nöpel, J.-A.; Rüdiger, F.; Paustian, D.; Braeutigam, P., 2022:** "Analysis of bisphenol A degradation in water by hydrodynamic cavitation based on optical and chemical methods", *Ultrasonics Sonochemistry*, Volume 83: 105950, <https://doi.org/10.1016/j.ultsonch.2022.105950>

**Mickler, M., 2014:** "In-line Analyse, Simulation und Vorhersage von flüssigen Mehrphasenströmungen in Extraktionskolonnen". Technische Universität Kaiserslautern, Department of mechanical engineering and process engineering, Dissertation.

**Munter, R., 2001:** „Advanced oxidation processes: current status and prospects“, *Proc Estonian Acad Sci Chem* 50:59–80.

**Nöpel, J.-A.; Zedler, P; Deggelmann, M.; Braeutigam, P.; Fröhlich, J.; Rüdiger, F., 2018:** "Experimental investigation of the bubble distribution and chemical reactions induced by hydrodynamic cavitation inside a reactor-a preliminary study", *Conference Proceedings 5th ICEFM, Munich, Germany*, pp. 679–684. (DOI:10.18726/2018\_2)

**Nöpel, J.-A.; Fröhlich, J.; Rüdiger, F., 2021:** "Experimental Investigation of Cavitation in a Jet Regarding Process Optimization", 11th International Symposium on Cavitation May, Daejeon, Korea.